JOURNAL OF Materials CHEMISTRY

Synthesis of scandia-stabilized zirconia *via* thermo-decomposition of precursor complexes

Ya-Wen Zhang, Jiang-Tao Jia, Chun-Sheng Liao and Chun-Hua Yan*

State Key Lab of Rare Earth Materials Chemistry and Applications & PKU-HKU Joint Lab on Rare Earth Materials and Bioinorganic Chemistry, Peking University, Beijing 100871, China. E-mail: chyan@chemms.chem.pku.edu.cn; Fax: +86-10-6275-4179

Received 2nd February 2000, Accepted 15th May 2000
Published on the Web 11th July 2000

Thermo-decomposition of precursor complexes was utilized to synthesize scandia-stabilized zirconia (ScSZ) with the composition $(Sc_2O_3)_{0.08}(ZrO_2)_{0.92}$. Mixtures of precursors with different contents of EDTA (ethylenediaminetetraacetic acid) were synthesized through a homogenous soft chemical process, enabling the influences of ligand content on the calcination and sintering behaviors to be investigated. ScSZ polycrystals in a predominately cubic and rhombohedral polyphase were obtained after sintering at 1300 °C for 6 h.

Introduction

In recent years, the development of fast oxide ion conductors has attracted the interest of many researchers, not only for their applications in chemical sensors[1] and electrochemical oxygen membranes,[2] but also for their potential in solid oxide fuel cells (SOFC).[3–5] Amongst these kinds of materials, rare earth-stabilized zirconia (RESZ) has been proven to possess relatively high ionic conductance and good mechanical properties at operating temperatures. In RESZ materials, scandia-stabilized zirconia (ScSZ) with the composition $(Sc_2O_3)_{0.08}(ZrO_2)_{0.92}$ shows the highest ionic conductivity (σ) of any zirconia-based electrolytes (0.32 S cm^{-1} at 1000 °C),[6–8] whereas the σ value of yttria-stabilized zirconia (YSZ) $(Y_2O_3)_{0.10}(ZrO_2)_{0.90}$ is only 0.13 S cm^{-1} at the same temperature. However, there are several drawbacks to scandia-stabilized zirconia: (i) it is a little difficult to prepare homogenous ScSZ materials,[9] (ii) its ionic conductivity and mechanical properties deteriorate with time to levels comparable to those of $(Y_2O_3)_{0.10}(ZrO_2)_{0.90}$,[8] and (iii) the cost of scandium oxide is much higher than that of yttrium oxide due to a lack of demand. For these reasons, YSZ has been accepted instead of ScSZ for commercial uses in oxygen sensors and SOFCs. Moreover, because ScSZ preparation requires a high sintering temperature and a long annealing time, and its measured crystal phase depends not only on the preparation method, but also on the sintering temperature, its physical properties have not been adequately clarified.

Generally, materials like ScSZ are prepared by conventional ceramic,[10,11] co-precipitation,[8,9] or solution–gelation (sol–gel) methods.[12] More recently, the thermo-decomposition of precursor complexes was successfully employed for the synthesis of $La_{0.3}Sr_{0.7}CoO_{3-\delta}$.[13] Our interest was in investigating whether this method could be utilized to prepare ScSZ bulk material under mild conditions, and understanding the calcination and sintering behaviors during the preparation. Due to the above-mentioned excellent features of $(Sc_2O_3)_{0.08}(ZrO2)_{0.92}$, we selected this material as our target and detail our studies on its synthesis and characterization in this work.

With the rapid progress in current scandium separation techniques,[14] it should not be too difficult to produce high purity scandium oxide on a large scale so that its cost can be reduced to an acceptable level if demand for commercial uses greatly increases. Therefore, it is reasonable to devote greater attention to the study of scandium-containing materials and the expansion of its fields of application.

Experimental

Synthesis

$Zr(EDTA)\cdot 4H_2O$. Synthesized by complexation of $ZrOCl_2\cdot 8H_2O$ (78 mmol) (Beijing Liulidian Chem. Plant of China, A.R.) with Na_2H_2EDTA (78 mmol) (Beijing Chem. Corp. of China, A.R.) in a beaker containing 400 ml deionized water under moderate heating. During the reaction, a small amount of white precipitation was produced due to the partial hydrolysis of ZrO_2^{2+}. After stirring for half an hour, the hot mother liquor was quickly filtered and cooled to room temperature, some white polycrystalline substances were gradually yielded on standing. Finally, the substances were filtered off, washed three times with deionized water and dried at 110 °C. Yield, 78%. Found: C, 26.80; H, 4.11; N, 6.16. Calc. for $C_{10}H_{20}N_2O_{12}Zr$: C, 26.60; H, 4.46; N, 6.20%. TG-DTA analysis, weight loss percentage and corresponding thermal effect: 15.8% [133–360 °C, weak (w) endothermic (endo.)], 48.9% [360–440 °C, very strong (vs) exothermic (exo.)], 6.78% [440–575 °C, exo. (w)].

$Sc(OH)_3\cdot 0.5H_2O$. Prepared as the starting material for the synthesis of the Sc–EDTA precursor complex. Sc_2O_3 (42 mmol) (Nonferrous Metals and Industry Corp. of Zhaoqing of Guangdong, 99.95%) was dissolved in excess concentrated $HClO_4$ solution (189 mmol) under continuous heating and stirring for about 8 h. As the solution cooled down, it was filtered and treated with excess 2.5 M NH_4HCO_3 solution, until complete precipitation occurred. The white precipitate was filtered off, washed three times with deionized water and dried at 110 °C. Yield, 98%. The scandium content was determined by the EDTA titration method using 0.75 M HCOOH–0.25 M HCOONa as a buffer solution, after the precipitate had been quantitatively dissolved in a dilute HCl solution. Found: H, 2.38; Sc, 43.6. Calc. for $H_4O_{3.5}Sc$: H, 3.84; Sc, 42.8. TG-DTA analysis: 13.9% [164–204 °C, endo. (m)], 11.4% [204–438 °C, endo. (w)].

Precursor complex mixture M1. $Sc(OH)_3\cdot 0.5H_2O$ and H_4EDTA in equal molar quantities were added to 300 ml deionized water and the solution stirred under mild heating. As the solution became transparent, a certain amount of

DOI: 10.1039/b000945h

$Zr(EDTA)\cdot 4(H_2O)$ in the molar ratio $Sc:Zr = 0.16:0.92$ was added, and gradually dissolved in the hot solution. Then the solution pH was adjusted to 6–7 by dropwise addition of a dilute ammonia solution. By almost evaporating the water solvent, **M1** was obtained and dried at 110 °C. Found: C, 27.89; H, 4.72; N, 8.03. Calc.: C, 28.36; H, 4.33; N, 7.23%. TG-DTA analysis: 11.7% [135–367 °C, endo. (w)], 50.4% [367–440 °C, exo. (vs)], 10.4% [44–600 °C, exo. (w)].

Precursor complex mixture M2. Prepared by following the previously described procedure for the synthesis of **M1**, but without the neutralization step. The final pH of the reaction mixture was about 4–5. Found: C, 28.45; H, 4.72; N, 6.93. Calc.: C, 28.59; H, 4.19; N, 6.67%. TG-DTA analysis: 7.89% [128–370 °C, endo. (w)], 53.6% [370–470 °C, exo. (vs)], 12.0% [470–600 °C, exo. (w)].

Precursor complex mixture M3. Prepared using the same synthetic procedure as that employed to prepare **M2**, except that EDTA was added quantitatively in the molar ratio $EDTA:Sc:Zr = 1.24:0.16:0.92$ in dissolving the scandium hydroxide. The final pH of the reaction mixture was *ca.* 2–3. Found: C, 29.03; H, 4.46; N, 7.12. Calc.: C, 30.3; H, 3.60; N, 7.68%. TG-DTA analysis: 6.66% [25–369 °C, endo. (w)], 53.5% [369–440 °C, exo. (vs)], 10.0% [440–600 °C, exo. (w)].

$(Sc_2O_3)_{0.08}(ZrO_2)_{0.92}$ powders P1, P2, and P3. Obtained by calcining certain amounts of the finely ground powders of **M1**, **M2** and **M3** in a corundum crucible for 2 h in stagnant air at different temperatures ranging from 600 to 1500 °C. Scandium and zirconium contents were determined by ICP-AES analysis, through completely dissolving weighed amounts of **P1**, **P2**, and **P3** in hot sulfuric acid. The determined stoichiometry is fully in agreement with the calculated composition ($Sc:Zr = 0.16:0.92$), this is also indirectly indicative that the empirical metal contents in **M1**, **M2** and **M3** agree with those calculated.

As described above, the elemental analysis results show that the experimental stoichiometry for **M1**, **M2**, **M3**, **P1**, **P2** and **P3** is in accord with that calculated. Thus, it is reasonable to assume that no volatile compounds exist in the products as a result of the synthesis processes described above.

In order to prepare dense specimens, **P1**, **P2** and **P3** obtained at 1000 °C were ground for 15 min in an agate mortar, then pressed into pellet specimens **S1**, **S2** and **S3**, respectively, with diameters of 10 mm under a pressure of 20 MPa. Then, **S1**, **S2** and **S3** were sintered under stagnant air at 1300 °C for 6–24 h.

Instruments

Elemental analysis of C, H and N was performed with a Carlo Erba 1102 elemental analyzer and metal contents were determined using an inductively coupled plasma atomic emission spectrometer (Leeman Lab. Inc.). TG-DTA analysis was carried out with a Du Pont 2100 thermal analyzer in air at a heating rate of 15 °C min^{-1}, using α-Al_2O_3 as a reference. XRD spectra of the sample pellets ($\phi = 5$ mm) were measured on a Rigaku D/max-2000 X-ray powder diffractometer using Cu-Kα radiation ($\lambda = 1.5408$ Å) at a scanning rate of 4° min^{-1} over the 2θ range 20–70°. BET specific surface area was determined using a ASAP 2010 analyzer (Micromeritics Co. Ltd.) at 77.5 K, with N_2 as the adsorbent over the pressure range 0.05–0.20P_0 (P_0: standard atmospheric pressure). Particle sizes were measured with a Coulter multisizer II, with the sample being dispersed in a 0.9% NaCl solution for several minutes under ultrasonic agitation. SEM images were taken on a fresh cross-section of the specimen with an AMARY 1910FE SEM under a working voltage of 20.0 kV.

Results and discussion

Calcination behavior

To understand the calcination behavior of the ScSZ material, first of all, it is very important to know the distribution dependence of the burnt organic impurities on the calcination temperature and time. The elemental results of thermo-decomposition of **M1**, **M2** and **M3** are listed in Table 1. It is noticeable that the amount of impurities decreases with increasing calcination temperature from 600 to 900 °C; above 900 °C, the total amount of impurities falls to below 0.5%, which means that the impurities have been almost completely removed. Such a temperature dependence was also found when synthesizing $La_{0.3}Sr_{0.7}CoO_{3-\delta}$ by the same method.[13] The calcination time dependence was examined for **M1** calcined at 800 °C. As can also be seen from Table 1, the impurity contents varied little on extending the calcination time from 1 to 16 h, this indicates that the contaminants cannot be reduced by just extending the calcination time at a relatively low temperature. Only at higher calcination temperature beyond 900 °C could the contaminants be reduced to trace amount so as to meet the requirements of a pure oxide material in this regard.

Secondly, it is necessary to know how the thermo-decomposition behaviors of the precursors complexes influence the solid state diffusion reaction and the particle properties of the calcined powders during calcination. The TG-DTA curves of **M1**, **M2** and **M3** have been determined and precisely analyzed, the thermo-decomposition data are summarized in the experimental section. Fig. 1 exhibits a typical combined TG-DTA run for **M1**. Similarly to the complex $Zr(EDTA)\cdot 4(H_2O)$, all three curves obtained show that **M1**, **M2** and **M3** follow a similar decomposition process, which can be roughly divided into two steps. The first is the escape of water molecules or water plus ammonia molecules below 370 °C, resulting in a weak endothermic peak. The second is the burning-out of the EDTA ligand in the temperature range of 370–600 °C, accompanied by a very strong shoulder exothermic peak and a huge amount of gas release, such as CO_2. The exothermal effect can be estimated from $\Delta H/gk$ (summarized in Table 2), which is equal to the area of a given thermal peak over the sample weight in a DTA curve, and is given by the following equation

$$\frac{\Delta H}{gk} = \frac{\int_{t1}^{t2} \Delta T \, \mathrm{d}t}{m}$$

where m is the reactant mass, ΔH the reaction enthalpy, g the geometric constant of the instrument used, k the thermal conductivity constant, ΔT the temperature difference, $t1$ the integral lower limit, and $t2$ the integral upper limit, respectively. This equation was derived from the following equation, initially suggested by Speil *et al.*,[15] and modified by Kerr and Kulp.[16]

$$\int_{t1}^{t2} \Delta T \, \mathrm{d}t = \frac{m(\Delta H)}{gk}$$

As can be seen from Table 2, the exothermic effect of the precursor complex mixtures is in the order **M1** < **M2** < **M3**, which is caused by the increasing organic component from **M1** to **M3**. Although this exothermic heat is much less than that provided by the external heating device, it is somewhat beneficial to the successive solid state diffusion reaction. With increasing organic content in the precursor complexes, the exothermic effect and the amount of gas released will increase over a short time. Consequently, this will result in a rapid increase in the number of defects, the enhancement of the specific surface area to the reactants and the improvement in surface reaction activity will, finally, lead to the polycrystalline phase appearing at relatively low calcination temperature. On

Table 1 Elemental analysis results of some impurities in the calcined $(Sc_2O_3)_{0.08}(ZrO_2)_{0.92}$ powders

	M1			M2			M3		
T/°C	C (%)	H (%)	N (%)	C (%)	H (%)	N (%)	C (%)	H (%)	N (%)
600	0.857	0.183	0.417	1.087	0.139	0.521	1.040	0.130	0.475
700	0.368	0.329	0.140	0.395	0.251	0.178	0.357	0.235	0.170
800	0.234	0.312	0.134	0.270	0.246	0.150	0.259	0.260	0.143
900	0.191	0.247	0.103	0.151	0.165	0.077	0.153	0.156	0.081
1000	0.102	0.106	0.068	0.123	0.108	0.066	0.118	0.115	0.072
1100	0.072	0.234	0.029	0.098	0.158	0.055	0.139	0.067	0.174
t*[a]/h	C (%)	H (%)	N (%)						
1	0.213	0.160	0.150						
2	0.234	0.312	0.134						
4	0.289	0.211	0.104						
8	0.249	0.167	0.158						
16	0.217	0.164	0.140						

[a] t*: different calcination times at 800 °C.

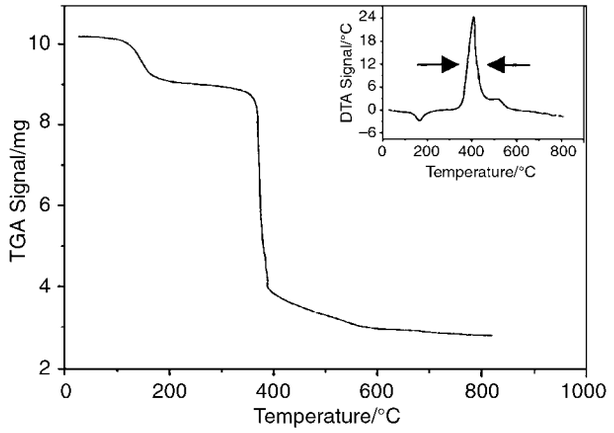

Fig. 1 Combined TG-DTA run of the precursor complex mixture **M1**.

the other hand, such effects as the exothermic reaction and the gas release are expected to have more or less impact on the particle properties of the calcined powders.

Fig. 2 displays the XRD patterns of **P1** at different calcination temperatures, from which, a very small amount

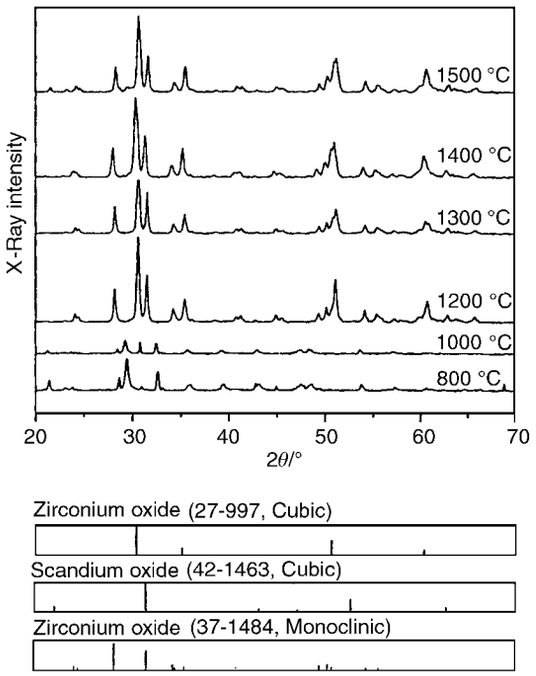

Fig. 2 XRD patterns of **P1** calcined at different temperatures for 2 h.

Table 2 Exothermic effect as a function of EDTA content in the precursor complex mixtures

	M1	M2	M3
$(\Delta H/gk)$/°C^2 mg^{-1}	143	146	156
Mol fraction of EDTA	0.46	0.50	0.54

of crystallized phase is evidenced below 1000 °C. Beyond 1000 °C, the crystallization process comes near to completion with the elevation of the calcination temperature, whereas the phase state of **P1** (a majority of cubic phase) is impure.

Fig. 3 depicts the dependence of the calcination temperature on the BET specific surface area, S, of **P1**, **P2** and **P3**. From this, it may be observed that S decreases non-linearly as the calcination temperature rises from 1100 to 1400 °C. It is postulated that this is due to the increase in the degree of particle aggregation and the decrease of grain defects, such as inner pores, with the elevation of calcination temperature. Below 1300 °C, S(**P1**) < S(**P2**) ≈ S(**P3**).

Fig. 4 shows the effect of calcination temperature on the median diameter d_{50} for **P1**, **P2** and **P3**. As the calcination temperature is increased from 1100 to 1300 °C, d_{50} of **P1** decreases gradually, while it tends to slightly increase for **P2** and **P3**. Perhaps this difference is caused by **P1** having many more metastable-stable large agglomerates than **P2** and **P3** and, at relatively high calcination temperature, some of the metastable-stable agglomerates gradually cracking into small ones. Below 1300 °C, d_{50}(**P1**) > d_{50}(**P2**) ≈ d_{50}(**P3**), which is the reverse of the S order, as expected.

As shown above, the differences in S and d_{50} of **P1**, **P2** and **P3** can be interpreted in terms of **P2** and **P3** having more small particles and grain defects than **P1**. However, above 1300 °C,

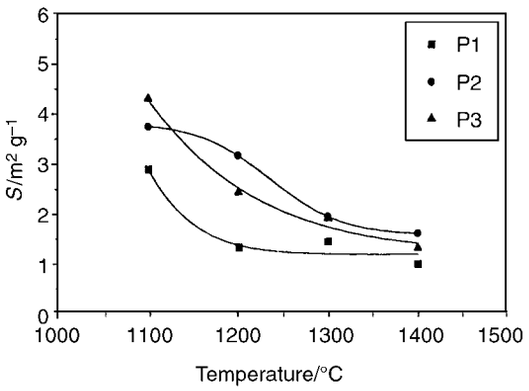

Fig. 3 Plots of BET specific surface area (S) of **P1**, **P2** and **P3** *vs.* calcination temperature.

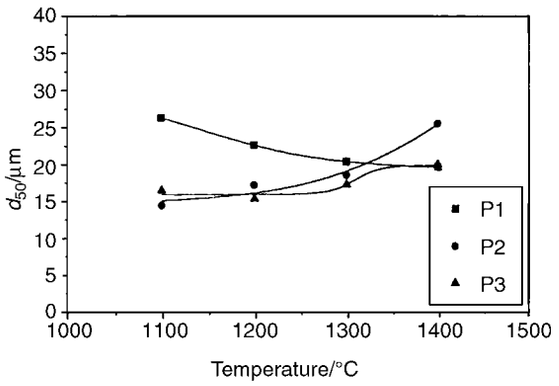

Fig. 4 Plots of median particle size (d_{50}) of **P1**, **P2** and **P3** *vs.* calcination temperature.

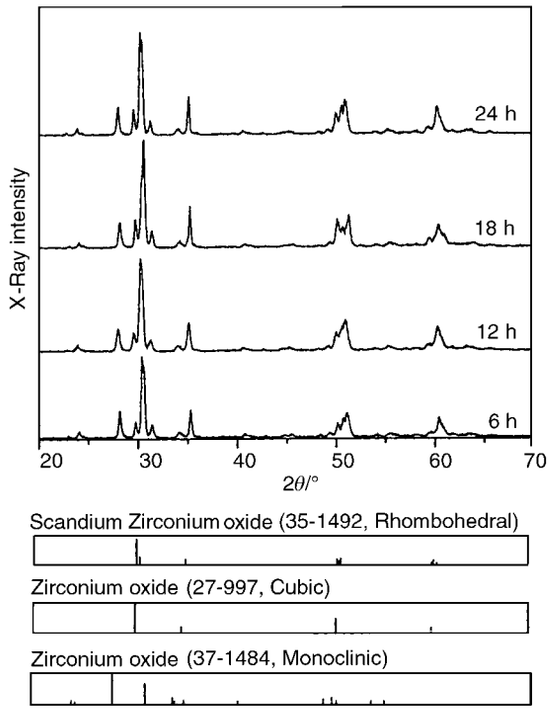

Fig. 5 XRD patterns of **S1** sintered at 1300 °C for different times.

the differences in S and d_{50} for **P1**, **P2** and **P3** are not prominent, possibly because of the similar agglomerates formed in each sample under much higher calcination temperatures.

Sintering behavior

As an example, Fig. 5 shows the sintering time dependence of the XRD patterns of **S1** at 1300 °C. As the sintering time was extended from 6 to 24 h, the intensities and positions of every observed peak changed little. This means that the crystalline phase state under these conditions can be attained in less than 6 h. According to some previous reports, the phase state of ScSZ in the rough composition $(Sc_2O_3)_{0.08}(ZrO_2)_{0.92}$ is quite confusing and depends not only on the preparation method, but also on the conditions. Ruh and Garrett found a single phase distorted fluorite tetragonal structure (prepared by conventional ceramic methods);[17] Badwal and co-worker reported a mixture of cubic and monoclinic phases,[18] or a t′-phase (tetragonal symmetry) with small splitting (prepared by co-precipitation method);[19] Mizutani *et al.* obtained a pure cubic phase (prepared by a sol–gel method);[12] Moghadam *et al.* observed a large increase in the β-rhombohedral phase from less than 5 to 15–20% on annealing at 800 °C for 200 h.[20] In this study, the phase state of $(Sc_2O_3)_{0.08}(ZrO_2)_{0.92}$ seems polyphasic, *i.e.* predominately a mixture of cubic and rhombohedral phases plus a little of the monoclinic phase.

Comparing Fig. 5 with Fig. 2, it can be seen that the relative intensities of the strongest diffraction peaks due to the monoclinic phase ($2\theta = 28.17°$) and cubic phase ($2\theta = 30.48°$) at 1300 °C sharply decrease due to the fact that the solid state reaction tends to be finished after **S1** has been sintered. In this case, many more monoclinic polycrystals have changed to cubic after sintering.

Fig. 6 shows SEM micrographs of cross-sections of **S1** (a), **S2** (b) and **S3** (c). In part initially caused by the differences in the particle properties of **P1**, **P2** and **P3**, as discussed previously, it can be observed from the micrographs that the degree of grain agglomeration in **S1** and **S2** is more severe than for **S3**.

Conclusions

As discussed above, the thermo-decomposition of precursor complexes is characteristic of soft chemical homogenous mixing of different metal ions and yields a large exothermic effect with a high volume of gases released in burning out the organic components. In this work, thermo-decomposition was successfully used to prepare $(Sc_2O_3)_{0.08}(ZrO_2)_{0.92}$ material with a short sintering time at a relatively low temperature. In conclusion, this method should be taken into consideration as a possible route for synthesizing many other composite oxides.

Acknowledgements

This work was supported by the NSFC (29525101 & 29832010), the State Key Project for Fundamental Research of MOST (G1998061300), the Training Project for Doctoral Student of MOE, and Founder Group Corporation Foundation of Peking University.

References

1 G.-y. Adachi and N. Imanaka, in *Handbook on the Physics and Chemistry of Rare Earths*, ed. K. A. Gschneider and L. Eyring,

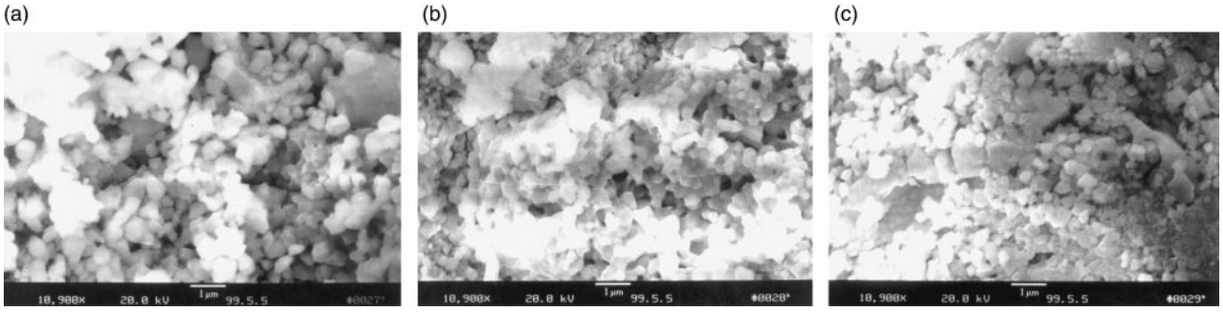

Fig. 6 SEM micrographs of **S1** (a), **S2** (b) and **S3** (c) sintered for 6 h at 1300 °C.

Elsevier Science B. V., North Holland, Amsterdam, 1995, vol. 21, p. 179.
2 V. V. Kharton, E. N. Naumovich and A. V. Nikolaev, *J. Membr. Sci.*, 1996, **111**, 149.
3 N. Q. Minh, *J. Am. Ceram. Soc.*, 1993, **76**, 563.
4 S. P. S. Badwal, M. J. Bannister and R. H. J. Hannink, in *Science and Technology of Zirconia V*, ed. S. P. S. Badwal, M. J. Bannister and R. H. J. Hannink, Technomic, Lancaster, PA, 1993, p. 631.
5 M. Dokiya, O. Yamamoto, H. Tagawa and S. C. Singhal, in *Solid Oxide Fuel Cells IV*, ed. M. Dokiya, O. Yamamoto, H. Tagawa and S. C. Singhal, The Electrochemical Society, Pennington, NJ, 1995, p. 657.
6 S. P. S. Badwal, *J. Mater. Sci.*, 1987, **22**, 4125.
7 F. M. Spiridonov, L. N. Popova and R. Ya. Popil'skii, *J. Solid State Chem.*, 1970, **2**, 430.
8 S. P. S. Badwal, *Solid State Ionics*, 1992, **52**, 23.
9 S. P. S. Badwal, F. T. Ciacchi, S. Rajerdran and J. Drennan, *Solid State Ionics*, 1998, **109**, 167.
10 D. W. Strickler and W. G. Carlson, *J. Am. Ceram. Soc.*, 1965, **48**(6), 286.
11 T. Ishii, T. Iwata and Y. Tajima, *Solid State Ionics*, 1992, **57**, 153.
12 Y. Mizutani, M. Tamura and M. Kawai, *Solid State Ionics*, 1994, **72**, 271.
13 R. H. E. Van Doorn, H. Kruidhof, A. Nijmeijer, L. Winnubst and A. J. Burggraaf, *J. Mater. Chem.*, 1998, **8**, 2109.
14 C. H. Yan, Y. Zhang, C. S. Liao, Z. J. Wei, Y. W. Zhang and B. G. Li, P.R.C. Patent no. 1127791A, 1991.
15 S. Speil, L. H. Berkelhamer, J. A. Pask and B. Davis, *U. S., Bur. Mines, Tech. Pap.*, 1945, 664.
16 P. F. Kerr and J. L. Kulp, *Am. Mineral.*, 1948, **33**, 387.
17 R. Ruh and H. J. Garrett, *J. Am. Ceram. Soc.*, 1977, **60**, 399.
18 S. P. S. Badwal, *J. Mater. Sci.*, 1983, **18**, 3230.
19 S. P. S. Badwal and J. Drennan, *Solid State Ionics*, 1992, **53–56**, 769.
20 F. K. Moghadam, T. Yamashita, R. Sinclair and D. A. Stevenson, *J. Am. Ceram. Soc.*, 1983, **66**, 213.